

Nonrelativistic Bound States in Quantum Field Theory*

Aneesh V. Manohar^a and Iain W. Stewart^a

^aDepartment of Physics, University of California at San Diego,
9500 Gilman Drive, La Jolla, CA 92093-0319

Nonrelativistic bound states are studied using an effective field theory. Large logarithms in the effective theory can be summed using the velocity renormalization group. For QED, one can determine the structure of the leading and next-to-leading order series for the energy, and compute corrections up to order $\alpha^8 \ln^3 \alpha$, which are relevant for the present comparison between theory and experiment. For QCD, one can compute the velocity renormalization group improved quark potentials. Using these to compute the renormalization group improved $\bar{t}t$ production cross-section near threshold gives a result with scale uncertainties of 2%, a factor of 10 smaller than existing fixed order calculations.

1. INTRODUCTION

Nonrelativistic bound states in QED and QCD provide an interesting and highly nontrivial problem to which effective field theory methods can be applied [1,2]. The QCD bound states we will consider are heavy $\bar{Q}Q$ states such as $\bar{t}t$ bound states or the Υ system. In QED, the classic examples are Hydrogen, muonium (μ^+e^-), and positronium. Each of these systems has three important scales, m the fermion mass, mv the fermion momentum, and mv^2 , the fermion energy. (For Hydrogen and muonium, m is the electron mass or the reduced mass of the two particles.) The velocity v is of order the coupling constant (α_s or α), and we will only consider the case $v \ll 1$, $mv^2 \gg \Lambda_{\text{QCD}}$ so that nonperturbative effects are small.

Multiscale problems with widely separated scales are well suited for study using effective field theories. For example, if the problem has the scales $m_1 \gg m_2 \gg m_3 \dots$, one first starts with the theory above m_1 , and matches to an effective theory below m_1 in which only modes with masses much smaller than m_1 are retained. The effective theory is then scaled using the renormalization group to the next scale m_2 . At this point, particles with mass m_2 are integrated out to con-

struct a new effective theory, and so on. The complicated multiscale computations of the original theory are reduced to a number of simpler single scale computations of matching and running in the effective theory. The effective theory method also allows one to sum logarithms of the ratio of mass scales $\ln m_i/m_{i+1}$ using the renormalization group evolution between m_i and m_{i+1} .

The goal is to correctly separate the scale m , mv and mv^2 for nonrelativistic bound state problems using an effective field theory, and to sum large logarithms using the renormalization group. The large logarithms in this case are $\ln p/m$, $\ln E/m$ and $\ln p/E$ which are proportional to $\ln v$, and lead to $\ln \alpha$ contributions to bound state energies. Furthermore, for QCD, the effective theory also determines the scale of the strong coupling constant, i.e. whether one should use $\alpha_s(m)$, $\alpha_s(mv)$ or $\alpha_s(mv^2)$. The nonrelativistic effective theory, NRQCD/NRQED, has been studied extensively in the past [1–17]. What is new is the precise formulation of the effective theory, and the way in which the renormalization group is scaling is implemented.

The results presented here will be applied to the study of $\bar{t}t$ production in the threshold region. There is a large ratio of scales, $m_t \sim 175$ GeV, $m_tv \sim 26$ GeV and $m_tv^2 \sim 4$ GeV, where $v \sim 0.15$ is the typical velocity in the nonrelativistic bound state. Clearly $\alpha_s \ln v$ is not small,

*UCSD/PTH 00-27. Talks presented at Lattice 2000 and SPIN 2000

and summing logarithms is important in this case.

The results are also useful in QED. While $\alpha \ln \alpha$ is small, it is important to compute to high orders because the experiments have high precision. The Hydrogen Lamb shift of 1057.845 MHz is known to an accuracy of 9 KHz [18], the Hydrogen hyperfine splitting is measured to be 1420.405 751 766 7(9) MHz [19], and the muonium hyperfine splitting is 4463.302 776(55) MHz [20]. The binding energy of Hydrogen, $m_e \alpha^2 / 2$ is 2×10^{10} MHz, so the experimental error in the Lamb shift of 10 ppm is a part in 10^{12} of the binding energy. We will be able to compute corrections of order $m_e \alpha^8 \ln^3 \alpha / (4\pi)^2 \sim 5$ KHz to the Lamb shift, which are relevant for the present comparison between theory and experiment. [The counting of 4π factors for bound states is a little different than the conventional counting [21]. Potential loops give powers of α whereas soft and ultrasoft loops give powers of $\alpha / (4\pi)$.]

A detailed comparison of theory and experiment for QED can be found in Refs. [22–24].

2. NEW RESULTS

There are many interesting new results that have been obtained for QED and QCD [11–15, 25–28]. For QED, one finds a universal description of $\ln \alpha$ terms. A single renormalization group equation gives the Lamb shift, hyperfine splitting and decay widths for Hydrogen, muonium and positronium. The renormalization group method allows us to compute for the first time the $\alpha^8 \ln^3 \alpha$ Lamb shift in positronium and the $\alpha^8 \ln^3 \alpha$ Lamb shift in Hydrogen and muonium including recoil corrections. It also resolves a controversy in the literature about the $\alpha^8 \ln^3 \alpha$ Hydrogen Lamb shift in the limit $m_p \rightarrow \infty$.

The renormalization group method allows one to understand the structure of the QED perturbation series, and why the $\ln \alpha$ corrections terminate. The leading order series has a single term that contributes at order $\alpha^5 \ln \alpha$ to the energy, and the next-to-leading order series terminates after three terms, $\alpha^6 \ln \alpha$, $\alpha^7 \ln^2 \alpha$, and $\alpha^8 \ln^3 \alpha$. One also finds some infinite series of terms in QED, but they have the form $(\alpha^3 \ln^2 \alpha)^n$, rather

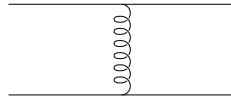


Figure 1. A potential gauge boson exchange. The typical momentum and energy transferred are mv and mv^2 .

than $(\alpha \ln \alpha)^n$.

In QCD, one is able to sort out the scales for α_s , and decide whether the strong coupling is $\alpha_s(m)$, $\alpha_s(mv)$, or $\alpha_s(mv^2)$. We also obtain the renormalization group improved computations of the bound states potentials in QCD. There are numerous applications of these results, and I will show an example of the dramatic improvement one obtains for the $\bar{t}t$ production cross-section near threshold [27, 28].

3. THE PROBLEM

The basic problem can be seen by drawing a few Feynman diagrams. A typical gauge boson exchange in the t channel such as Fig. 1 has momentum transfer of order $p \sim mv$. A wavefunction graph or radiated gauge boson graph such as Figs. 2 have gauge boson momenta of order $E \sim mv^2$. More interesting diagrams such as those in Figs. 3 involve gauge bosons with momenta of order p and order E . In a graph such as Fig. 4, the vacuum polarization insertions make the effective coupling of the two gluons $\alpha_s(mv)$ and $\alpha_s(mv^2)$ respectively. One result which should be clear from Fig. 4 is that graphs can involve $\alpha_s(mv)$ and $\alpha_s(mv^2)$ *simultaneously*. We will return to this important point later on.

4. MOMENTUM REGIONS AND DEGREES OF FREEDOM

The Feynman integrals in the full theory can be evaluated using the threshold expansion [29]. The important momentum regions (in Feynman gauge) are referred to in the literature as hard ($E \sim m$, $p \sim m$), potential ($E \sim mv^2$, $p \sim mv$),

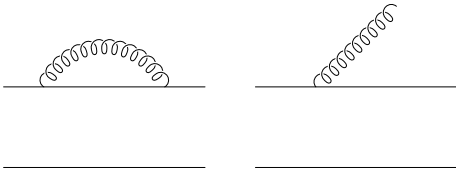


Figure 2. Graphs containing ultrasoft photons, with energy and momentum of order mv^2 .

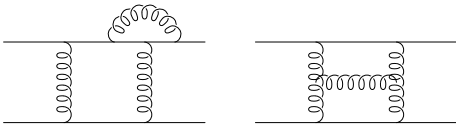


Figure 3. Graphs containing gauge bosons carrying momentum of order mv and mv^2 .

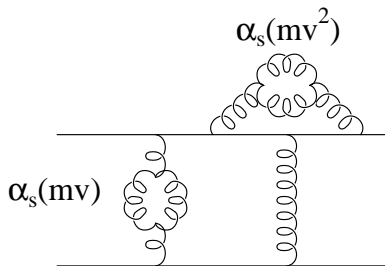


Figure 4. An example of a graph involving both $\alpha(mv)$ and $\alpha(mv^2)$.

ultrasoft ($E \sim mv^2$, $p \sim mv^2$) and soft ($E \sim mv$, $p \sim mv$). The threshold expansion momentum regions are often used to describe bound state computations; however it is important to note that *the threshold expansion is not an effective field theory*. To construct an effective field theory, one needs to include only modes that can be on-shell. The effective theory therefore has nonrelativistic fermions (which are potential modes), and soft and ultrasoft gauge boson modes. The hard fermion and gauge boson momentum regions, the soft fermion momentum region, and the potential gauge boson momentum region do not require modes in the effective theory.

The desired effective theory is valid for energies and momenta much smaller than the fermion mass m . One can try expanding in powers of E/m and p/m as in heavy quark effective theory, so that the expansion parameter is $1/m$. For example, the dispersion relation $E = \sqrt{\mathbf{p}^2 + m^2}$ gives terms in the Lagrangian of the form

$$L = \psi^\dagger \left(E - \frac{\mathbf{p}^2}{2m} + \frac{\mathbf{p}^4}{8m^3} + \dots \right) \psi. \quad (1)$$

The lowest order propagator is $1/(E + i\epsilon)$, which gives $\theta(t)$ in position space. This is the static propagator of HQET: fermions propagate forward in time, but do not move in space. This propagator is acceptable for some calculations involving heavy quarks. For example, one can compute the static potential between fixed sources using this propagator. However, for $\bar{t}t$ production, the quarks are produced at the same point, and they remain at the same point for all time if the static propagator is used. This is too singular, and the HQET expansion breaks down. In general, it is essential for treating nonrelativistic bound states that the heavy fermions move. For this to occur, the lowest order propagator should be $1/(E - \mathbf{p}^2/2m + i\epsilon)$, so that E and $\mathbf{p}^2/2m$ are of the same order in the effective theory power counting. This implies that the $1/m$ expansion cannot be used; instead one must use an expansion in powers of v , where E and $\mathbf{p}^2/2m$ are both of order v^2 [1,2].

The effective theory expansion parameter is the velocity v , and formally, α must also be treated as order v . Thus order α^2 radiative corrections to

the leading term are just as important as order v^2 relativistic corrections. The effective theory below the scale m has:

- Nonrelativistic fermions with propagator

$$\frac{1}{E - \mathbf{p}^2/2m + i\epsilon}$$

- Ultrasoft gauge bosons coupled via interactions that are multipole expanded [6].
- Potentials $V(\mathbf{p}, \mathbf{p}')$ for the scattering of an incoming Q and \bar{Q} with momenta \mathbf{p} and $-\mathbf{p}$ to outgoing Q and \bar{Q} with momenta \mathbf{p}' and $-\mathbf{p}'$.
- Soft gauge bosons. The importance of introducing soft fields in the effective theory was first pointed out by Griesshammer [30].

The effective theory has two different gauge boson fields, soft bosons and ultrasoft bosons. This does not lead to any double counting if graphs are evaluated in dimensional regularization.

The static theory is not the $m \rightarrow \infty$ limit or the $v \rightarrow 0$ limit of the effective theory. For this reason, the static potential and the effective theory potential are not equal.

5. POWER COUNTING

The power counting parameter of the effective theory is the velocity v . If one expands the dispersion relation as in Eq. (1), then E and $\mathbf{p}^2/2m$ are both of order v^2 , and $\mathbf{p}^4/8m^3$ is of order v^4 , i.e. of order v^2 relative to the leading term.

The potential $V(\mathbf{p}, \mathbf{p}')$ also has an expansion in powers of v . The leading term is the Coulomb potential, $V(\mathbf{p}, \mathbf{p}') \propto \alpha/|\mathbf{k}|^2$, where $k = \mathbf{p}' - \mathbf{p}$ is the momentum transfer. Since momentum is of order mv , the Coulomb potential is naively of order α/v^2 . However, the potential is a four-fermion operator, whereas the kinetic energy is a two-fermion operator. This leads to an additional factor of v from the power counting factors for the fields, so that the Coulomb potential is of order α/v in the effective theory. One can then determine the power counting for all the other

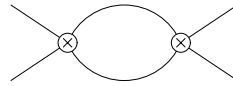


Figure 5. An iteration of two potentials in the effective theory.

potentials by comparing with the Coulomb potential. The hyperfine interaction $\propto \alpha \mathbf{S}_1 \cdot \mathbf{S}_2/m^2$ is generated by one-photon exchange, and is of order v^2 relative to the Coulomb interaction, so it is of order αv in the power counting, as are the spin-orbit, tensor and contact (Darwin) interactions. At one-loop, there are also potentials that are proportional to odd-powers of \mathbf{k} . The first such potential is proportional to $\alpha^2/|\mathbf{k}|$, and is of order $\alpha^2 v^0$ in the power counting.

A loop graph such as Fig. 5 of the time-ordered product of two potentials of order $\alpha^{a_1} v^{b_1}$ and $\alpha^{a_2} v^{b_2}$ is of order $\alpha^{a_1+a_2} v^{b_1+b_2}$. One can now see that the static potential differs from the $m \rightarrow \infty$ or $v \rightarrow 0$ limit of the effective theory potentials. For example, the loop graph of Fig. 5 with one $1/(m|\mathbf{k}|)$ and one Coulomb potential is of order $\alpha^2 v^0 \times \alpha/v = \alpha^3/v$, and is of the same order in v as the Coulomb potential. The two particle intermediate state propagator $1/(E - \mathbf{p}^2/2m) = 2m/(2mE - \mathbf{p}^2)$ produces a factor of m in the numerator, that cancels the $1/m$ at the vertex. In the static theory, the $1/(m|\mathbf{k}|)$ potential is set to zero before the loop integration, so that the graph of Fig. 5 is not present in the static theory. As a result, the NRQCD potential [26] differs from the static potential.

6. MATCHING CONDITIONS

The method of calculating matching conditions is the same as in any effective theory. One computes the graphs in the full theory at the scale $\mu = m$, and subtracts the corresponding graphs in the effective theory. The graph in Fig. 6 gives the matching condition for the fermion potential.

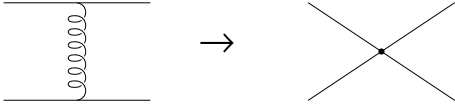


Figure 6. Tree-level matching for the potential.

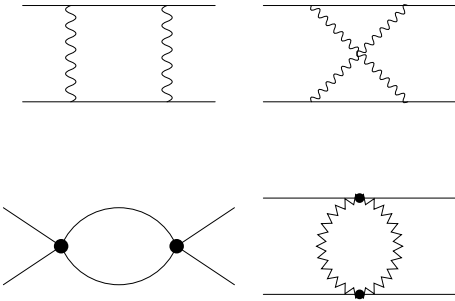


Figure 7. One-loop matching for the potential in QED. The first line gives examples of the full theory graphs. The second line gives examples of effective theory graphs: an iteration of two potentials, and a soft photon graph. The difference of the two sets of graphs gives the one-loop correction to the potential.

The full theory amplitude,

$$\frac{[\bar{u}(\mathbf{p}')\gamma^\mu u(\mathbf{p})][\bar{u}(-\mathbf{p}')\gamma_\mu u(-\mathbf{p})]}{(\mathbf{p} - \mathbf{p}')^2} \quad (2)$$

is expanded in powers of \mathbf{p}, \mathbf{p}' , to give the potential in the effective theory. At one-loop, the difference of the full theory and effective theory graphs in Fig. 7 give the one-loop corrections to the matching potential. The only difference at this stage between Hydrogen and positronium is that there are annihilation contributions to the positronium potential from graphs such as Fig. 8. The graphs can have an imaginary part, that give the positronium decay width.



Figure 8. Annihilation contributions to the positronium potentials. The second graph has an imaginary part. [There is also a one-loop crossed box in the annihilation channel.]

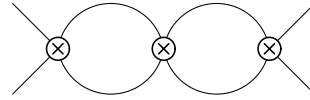


Figure 9. An ultraviolet divergent two-loop graph involving the iteration of three potentials.

7. RENORMALIZATION GROUP EVOLUTION

The nonrelativistic bound state system has three important mass scales, m , mv and mv^2 .

7.1. Two-stage running

The conventional method of implementing the renormalization group is as follows

- Start at $\mu = m$
- Scale μ from m to mv
- Integrate out the soft modes at mv
- Scale μ from mv to mv^2

This is referred to as the two-stage method, because there are two-stages of renormalization group evolution. Consider a loop graph involving time-ordered products of potentials, such as Fig. 9. This graph contains a logarithm of the form $\ln \sqrt{mE}/\mu$. When μ is set to mv , this logarithm has the form $\ln \sqrt{E/mv^2}$, and is small. Thus the logarithms in the graph are summed by renormalization group evolution of μ from m to mv .

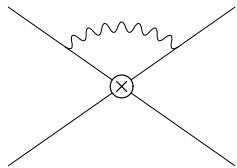


Figure 10. One-loop ultraviolet photon renormalization of the potential.

The graph in Fig. 10 involving an ultraviolet photon exchange contains a logarithm of the form $\ln E/\mu$. The μ in this ultraviolet graph is scaled all the way down (in two stages) to mv^2 , at which point the logarithm is $\ln E/mv^2$, and also small.

However, this two-stage method of implementing the renormalization group turns out to be incorrect for nonrelativistic bound states. The reason is that the scales mv and mv^2 are correlated— one cannot be varied independently of the other. Instead one needs to use an alternative one-stage scaling procedure.

7.2. One-stage running

In one stage running, one introduces two different μ parameters, μ_S and μ_U [11]. In dimensional regularization in $4 - 2\epsilon$ dimensions, the soft photon coupling is multiplied by μ_S^ϵ , the ultraviolet photon coupling by μ_U^ϵ , and the potentials by $\mu_S^{2\epsilon}$. Note that this is only possible because we have two different photon fields to represent the soft and ultraviolet photons in the effective theory. Then

- Set $\mu_S = mv$, $\mu_U = mv^2$
- Start at $\nu = 1$ and scale to $\nu = v$.

This procedure is referred to as the velocity renormalization group, because one runs in velocity ν rather than momentum [11]. The logarithms in Figs. 9 and 10 are now $\ln \sqrt{mE}/mv$ and $\ln E/mv^2$, which are minimized when $\nu = v$. Thus this method also minimizes logarithms in the diagrams, and sums them by renormalization group evolution.

The difference between the two renormalization group methods can be seen in Fig. 11 [25]. In

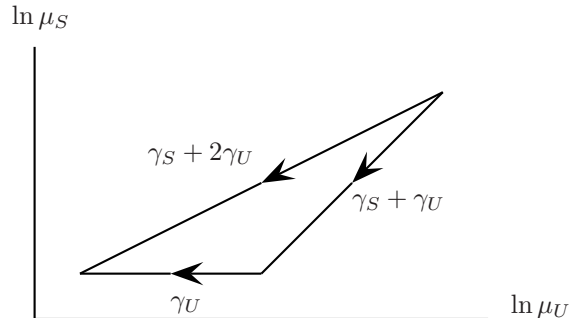


Figure 11. Paths in the (μ_U, μ_S) plane for one-stage and two-stage running.

two-stage running, there is only a single μ , so that $\mu_S = \mu_U = \mu$, and they are lowered together from m to mv . At this point, the soft modes are integrated out, and μ_U for the ultraviolet modes is lowered to mv^2 . The integration path in Fig. 11 is along the lower edges of the triangle. In one-stage running, the integration path is along the diagonal. It is convenient to define two anomalous dimensions, γ_S and γ_U by taking the derivatives of Green's functions with respect to $\ln \mu_S$ and $\ln \mu_U$, respectively. One can show by explicit calculation that

- The two paths give different answers. The integration is path dependent because $\nabla \times \gamma \neq 0$.
- One-stage running using the velocity renormalization group agrees with explicit QED calculations at order $\alpha^3 \ln^2 \alpha$, $\alpha^7 \ln^2 \alpha$ and $\alpha^8 \ln^3 \alpha$.

The moral is that for nonrelativistic bound states, one should run in velocity rather than momentum.

The difference between the two integration methods can be made more precise. In the two-stage method, one first integrates $\gamma_S + \gamma_U$ from $\mu = m$ to $\mu = mv$, and then integrates γ_U from $\mu = mv$ to $\mu = mv^2$. In the one-stage method, one integrates $\gamma_S + 2\gamma_U$ (since $\ln \mu_U$ runs twice as

fast as $\ln \mu_S$) from $\nu = 1$ to $\nu = v$. If the anomalous dimensions are constant, the two methods give

$$(\gamma_S + \gamma_U) \ln \frac{mv}{m} + \gamma_U \ln \frac{mv^2}{mv} \quad \text{two-stage}$$

$$(\gamma_S + 2\gamma_U) \ln v \quad \text{one-stage}$$

and agree with each other. However, in general anomalous dimensions are not constant, but can depend on coupling constants V_i , that themselves run. As a result, one finds that the $\ln v$ terms agree, but the higher order terms differ. For example, consider a $\ln^2 v$ term that depends on the product of γ_S and γ_U . For two-stage running, the contribution is proportional to $\gamma_S \gamma_U + 0\gamma_U = \gamma_S \gamma_U$ from the two pieces of the path. For one-stage running, the contribution is $\gamma_S (2\gamma_U)$, which differs by a factor of two. Similarly, a $\gamma_S \gamma_U^2 \ln^3 v$ contribution differs by a factor of four, and so on.

8. RUNNING POTENTIALS

The running potential $V(\mathbf{p}, \mathbf{p}')$ has an expansion

$$V(\mathbf{p}, \mathbf{p}') = V^{(-1)} + V^{(0)} + V^{(1)} + V^{(2)} + \dots \quad (3)$$

where $V^{(n)}$ is of order v^n in the velocity power counting. The first three terms in the expansion have the form

$$\begin{aligned} V^{(-1)} &= \frac{U_c}{\mathbf{k}^2}, \\ V^{(0)} &= \frac{U_k}{|\mathbf{k}|}, \\ V^{(1)} &= U_2 + U_s \mathbf{S}^2 + \frac{U_r(\mathbf{p}^2 + \mathbf{p}'^2)}{2\mathbf{k}^2} \\ &\quad - \frac{i\mathbf{U}_\Lambda \cdot (\mathbf{p}' \times \mathbf{p})}{\mathbf{k}^2} \\ &\quad + U_t \left(\boldsymbol{\sigma}_1 \cdot \boldsymbol{\sigma}_2 - \frac{3\mathbf{k} \cdot \boldsymbol{\sigma}_1 \mathbf{k} \cdot \boldsymbol{\sigma}_2}{\mathbf{k}^2} \right), \end{aligned} \quad (4)$$

where $V^{(0)} \sim 1/m$, and $V^{(1)} \sim 1/m^2$. In QCD, each of the coefficients can be written as $U \rightarrow U^{(1)}1 \otimes 1 + U^{(T)}T^A \otimes \bar{T}^A$, where 1 and T^A/\bar{T}^A are color matrices acting on the quark/antiquark lines. The anomalous dimensions for the coefficients U_c-U_t have been computed, and the details are given in Refs. [12–14]. The renormalization group improved static potential was computed in Ref. [31]. An important point to note

Table 1

Numerical values for the $\bar{t}t$ singlet potentials. The values at $\nu = 1$ are the matching values at $\mu = m_t$. The values at $\nu = v$ are the velocity renormalization group improved values, where $v = 0.14$ has been used.

Coefficient	$\nu = 1$	$\nu = v$
$U_c^{(s)}$	-1.81	-2.47
$mU_k^{(s)}$	-0.36	-0.03
$m^2U_r^{(s)}$	-1.81	-1.49
$m^2U_2^{(s)}$	0	0.63
$m^2U_s^{(s)}$	0.60	0.53
$m^2U_\Lambda^{(s)}$	0.15	0.16
$m^2U_t^{(s)}$	2.71	3.11

is that graphs can involve both soft and ultrasoft gluons, so that the anomalous dimensions involve both $\alpha_s(mv)$ and $\alpha_s(mv^2)$. As an example, the running of $U_2^{(1)}$ is given by

$$\begin{aligned} m^2U_2^{(1)}(\nu) &= \frac{14C_1}{3} \alpha_s(mv) \alpha_s(m) \ln \left(\frac{mv}{m} \right) \\ &\quad - \frac{32\pi C_1}{3\beta_0} \alpha_s(m) \ln \left[\frac{\alpha_s(mv)}{\alpha_s(mv^2)} \right] \end{aligned} \quad (5)$$

where $C_1 = 2/9$ for QCD. Note that Eq. (5) depends on $\alpha_s(m)$, $\alpha_s(mv)$, and $\alpha_s(mv^2)$. The running coefficients in the singlet channel ($U^{(s)} = U^{(1)} - C_F U^{(T)}$) for $\bar{t}t$ production are presented in Table 1. The renormalization group improved coefficients U_r and U_2 differ significantly from their matching values, because they depend on the ultrasoft scale through $\alpha_s(mv^2)$. The other coefficients only have a soft anomalous dimension, and do not run as much.

The renormalization group improved potentials can be used to calculate the renormalization group improved cross-section for $\bar{t}t$ production in the threshold region. Fig. 12 shows a sample fixed order calculation of R , the ratio of $\sigma(e^+e^- \rightarrow \bar{t}t)/\sigma(e^+e^- \rightarrow \mu^+\mu^-)$ [32]. The scale uncertainty is of order 20%. The renormalization group improved version of the results is shown

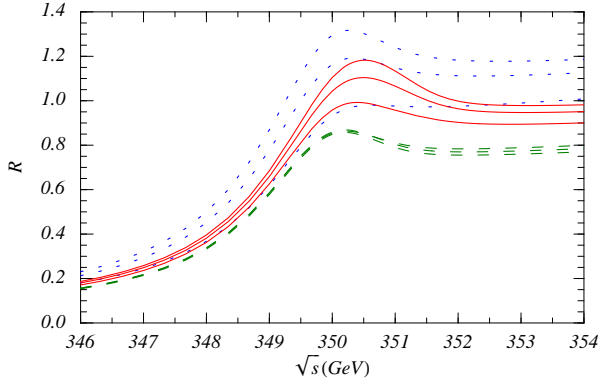


Figure 12. Fixed order computation of $\bar{t}t$ production near threshold. The curves are LO (dotted), NLO (dashed) and NNLO (solid.) Uses the $1S$ mass-scheme [33–35]

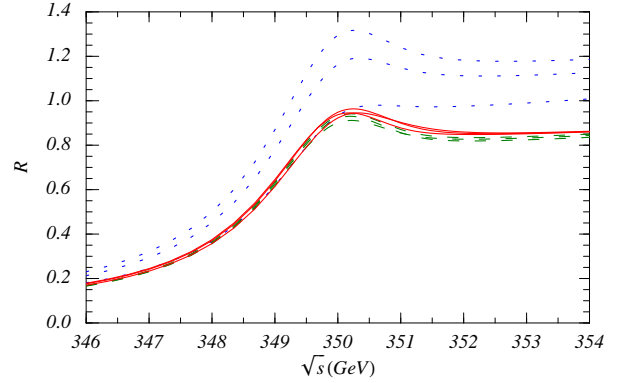


Figure 13. Renormalization group improved computation of $\bar{t}t$ production near threshold. The curves are LL (dotted), NLL (dashed) and NNLL (solid.). Uses the $1S$ mass-scheme [33–35]

in Fig. 13. There is a dramatic reduction in the scale uncertainty, which is now around 2%, as well as an improvement in convergence for the normalization. The small theoretical uncertainty means that an accurate measurement of the cross-section can be used to study new physics. For example, a standard model Higgs boson of mass around 115 GeV changes the cross-section by $\sim 5\%$, and is measurable.

9. QED

The velocity renormalization group method gives very interesting and important results when applied to QED [15]. The basic potentials we will need for QED are summarized in Table 2. The last column gives the contribution to the bound state energy levels due to the given potential. The fourth column gives the order of a given potential, treating v as order α . Since the Coulomb potential is of order unity, one finds the obvious result that the Coulomb potential must be summed to all orders, and cannot be treated as a perturbation. The potentials $V^{(-1)}$, $V^{(1)}$, $V^{(3)}$, are first generated at tree-level, and are of order α , whereas the potentials $V^{(0)}$, $V^{(2)}$, $V^{(4)}$, are first generated at one-loop, and are of order α^2 .

The bound state energy levels can be deter-

mined to order α^4 by computing the matrix elements of $V^{(0)}$ and $V^{(1)}$ between Coulomb wavefunctions. Time-ordered products of two potentials, such as $T[V^{(0)}V^{(0)}]$, $T[V^{(0)}V^{(1)}]$ and

Table 2

Table of potentials for QED. The first column is the potential, the second gives typical terms in the potential, the third gives the power counting in α and v , the fourth gives the order in the v counting scheme when $v \sim \alpha$, and the fifth gives the contribution of the potential to the bound state energy.

		Power Counting	Order	E
$V^{(-1)}$	$\frac{\alpha}{\mathbf{k}^2}$	$\frac{\alpha}{v}$	1	α^2
$V^{(0)}$	$\frac{\alpha}{m \mathbf{k} }$	α^2	α^2	α^4
$V^{(1)}$	$\frac{\alpha}{m^2}, \frac{\alpha \mathbf{S}^2}{m^2}$	αv	α^2	α^4
$V^{(2)}$	$\frac{\alpha \mathbf{k} }{m^3}$	$\alpha^2 v^2$	α^4	α^6
$V^{(3)}$	$\frac{\alpha \mathbf{k}^2}{m^4}$	αv^3	α^4	α^6
\vdots	\vdots	\vdots	\vdots	\vdots

$T[V^{(1)}V^{(1)}]$ first contribute at order α^6 . In principle, to obtain the energy levels to order α^4 , one also needs the one- and two-loop matching corrections to the Coulomb potential. However, such corrections vanish in QED. As a result, the first correction to the order α^2 binding energy is of order α^4 , and is given by the matrix element of $V^{(0)} + V^{(1)}$. There are no order α^3 corrections to the energy levels in QED.

Define the leading and next-to-leading order anomalous dimensions of a potential to be the anomalous dimension from graphs at one and two higher orders in α than the potential itself. For $V^{(-1)}$ and $V^{(1)}$ which are of order α , the leading order anomalous dimension is of order α^2 , and the next-to-leading order anomalous dimension is of order α^3 . For $V^{(0)}$ which is of order α^2 , the leading order anomalous dimension is of order α^3 , and the next-to-leading order anomalous dimension is of order α^4 . Since different terms in the potential are of different orders in α , the terms leading and next-to-leading order are not related to the number of loops.

Integrating the renormalization group equations for $V^{(0)}$ and $V^{(1)}$ using the leading order anomalous dimension gives a series of the form

$$\alpha(1 + \alpha \ln \alpha + \alpha^2 \ln^2 \alpha + \alpha^3 \ln^3 \alpha + \dots),$$

which contributes

$$\alpha^4(1 + \alpha \ln \alpha + \alpha^2 \ln^2 \alpha + \alpha^3 \ln^3 \alpha + \dots)$$

to the energy. Integrating the next-to-leading order anomalous dimensions gives

$$\alpha^4 \alpha(1 + \alpha \ln \alpha + \alpha^2 \ln^2 \alpha + \alpha^3 \ln^3 \alpha + \dots)$$

terms in the energy. The next-to-next-to-leading anomalous dimension gives

$$\alpha^4 \alpha^2(1 + \alpha \ln \alpha + \alpha^2 \ln^2 \alpha + \alpha^3 \ln^3 \alpha + \dots),$$

terms in the energy, which are the same order as those obtained by using the leading order anomalous dimension for the $V^{(2)}$ and $V^{(3)}$ potentials which first contribute at order α^6 . Thus one can compute the

$$\begin{array}{llll} \alpha^5 \ln \alpha & \alpha^6 \ln^2 \alpha & \alpha^7 \ln^3 \alpha & \dots \\ \alpha^6 \ln \alpha & \alpha^7 \ln^2 \alpha & \alpha^8 \ln^3 \alpha & \dots \end{array}$$

series in the energy using $\gamma_{\text{LO}}, \gamma_{\text{NLO}}$ for $V^{(0,1)}$.

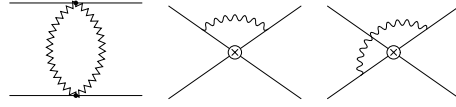


Figure 14. One-loop running of $V^{(1)}$ in QED. The first graph has a soft photon, and the other graphs have ultrasoft photons and a potential.

10. LEADING ORDER

The Coulomb potential and $V^{(0)}$ do not run in QED at leading and next-to-leading order, so one is left with the running of $V^{(1)}$. The anomalous dimensions are evaluated for a particle of mass m_1 and charge $-e$ interacting with a second particle of mass m_2 and charge Ze . Evaluating the graphs in Fig. 14 gives

$$\nu \frac{dU_2}{d\nu} = \frac{14Z^2\alpha^2}{3m_1m_2} + \frac{2\alpha}{3\pi} \left(\frac{1}{m_1} + \frac{Z}{m_2} \right)^2 U_c \quad (6)$$

where the first term is the soft contribution from Fig. 14a and the second is the ultrasoft contribution from Fig. 14b,c. Note that the ultrasoft contribution has been multiplied by two, since the anomalous dimension for the velocity renormalization group is $\gamma_S + 2\gamma_U$. The other coefficients in $V^{(1)}$ (U_r, U_s, U_Λ, U_t) have zero anomalous dimension at this order.

Since the Coulomb potential and α do not run in QED, one can combine the two terms,

$$\nu \frac{dU_2}{d\nu} = \gamma_0 U_c \quad (7)$$

which defines

$$\gamma_0 = \frac{2\alpha}{3\pi} \left(\frac{1}{m_1^2} + \frac{Z}{4m_1m_2} + \frac{Z^2}{m_2^2} \right). \quad (8)$$

γ_0 is a constant in QED since α does not run. Integrating Eq. (7) gives

$$U_2(\nu) = U_2(1) + \gamma_0 U_c \ln \nu, \quad (9)$$

where U_2 is evaluated at $\nu = v = \alpha$. Since γ_0 is a constant, $U_2(\nu)$ only has a $\ln \nu$ term, and terms of the form $\ln^n \nu$, with $n > 1$ vanish. As a

result, the leading order energy series Eq. (9) terminates after a single term, so one has an $\alpha^5 \ln \alpha$ contribution to the energy, but the $\alpha^6 \ln^2 \alpha$, etc. terms vanish. At low orders, the absence of terms other than $\alpha^5 \ln \alpha$ in the leading order series has been noticed before by an explicit examination of Feynman graphs. This is the first general proof that all the terms beyond $\alpha^5 \ln \alpha$ in the leading order series vanish

The matrix element of U_2 gives the energy shift

$$\begin{aligned} \Delta E &= \langle U_2(\nu) \rangle \\ &= \gamma_0 U_c \ln \nu |\psi(\mathbf{0})|^2 \\ &= -\frac{8Z^4 \alpha^5 m_R^3}{3\pi n^3} \left(\frac{1}{m_1^2} + \frac{Z}{4m_1 m_2} + \frac{Z^2}{m_2^2} \right) \ln Z\alpha, \end{aligned} \quad (10)$$

where we have used

$$|\psi(\mathbf{0})|^2 = \frac{(m_R Z \alpha)^3}{\pi n^3} \quad (11)$$

for the nS state, and m_R is the reduced mass. This is the famous $\alpha^5 \ln \alpha$ correction to the Lamb shift first computed by Bethe, including all recoil corrections.

11. NEXT-TO-LEADING ORDER

At next-to-leading order, the anomalous dimension for $V^{(1)}$ is

$$\begin{aligned} \nu \frac{dU_{2+s}}{d\nu} \Big|_{\text{NLO}} &= \rho_{ccc} U_c^3 + \rho_{cc2} U_c^2 (U_{2+s} + U_r) \\ &+ \rho_{c22} U_c \left(U_{2+s}^2 + 2U_{2+s} U_r + \frac{3}{4} U_r^2 - 5U_t^2 \mathbf{S}^2 \right) \\ &+ \rho_{ck} U_c U_k + \rho_{k2} U_k (U_{2+s} + U_r/2) \\ &+ \rho_{c3} U_c \left(U_3 + U_{3s} \mathbf{S}^2 + \frac{1}{2} U_{rk} \right), \end{aligned} \quad (12)$$

where $U_{2+s} = U_2 + U_s \mathbf{S}^2$, and the coefficients are

$$\begin{aligned} \rho_{ccc} &= -\frac{m_R^4}{64\pi^2} \left(\frac{1}{m_1^3} + \frac{1}{m_2^3} \right)^2, \\ \rho_{c22} &= -\frac{m_R^2}{4\pi^2}, \\ \rho_{cc2} &= -\frac{m_R^3}{8\pi^2} \left(\frac{1}{m_1^3} + \frac{1}{m_2^3} \right), \\ \rho_{c3} &= \frac{2m_R}{\pi^2}, \end{aligned}$$

$$\begin{aligned} \rho_{ck} &= \frac{m_R^2}{2\pi^2} \left(\frac{1}{m_1^3} + \frac{1}{m_2^3} \right), \\ \rho_{k2} &= \frac{2m_R}{\pi^2}. \end{aligned} \quad (13)$$

The anomalous dimension Eq. (12) can be integrated by substituting the leading order running, Eq. (9) for the coefficients on the right-hand side. Since only U_2 runs at leading order, the right hand side has at most a $\ln^2 \nu$, so that the integral has at most a $\ln^3 \nu$ term. This implies that the next-to-leading order series Eq. (9) terminates after the first three terms, $\alpha^6 \ln \alpha$, $\alpha^7 \ln^2 \alpha$, and $\alpha^8 \ln^3 \alpha$.

11.1. $\ln^3 \alpha$

The only term that contributes to the $\ln^3 \alpha$ correction is the U_2^2 term of Eq. (12). Integrating gives a contribution to $U_2(\nu)$ of the form

$$\frac{1}{3} \gamma_0^2 \rho_{c22} U_c^3(1) \ln^3 \nu, \quad (14)$$

which is spin-independent, and has no imaginary part. There is no contribution to the decay width or hyperfine splitting at this order. The Lamb shift at this order is obtained by multiplying Eq. (14) by the matrix element of the unit operator, $|\psi(\mathbf{0})|^2$, to give

$$\begin{aligned} \Delta E &= \frac{64m_R^5 \alpha^8 Z^6}{27\pi^2 n^3} \ln^3(Z\alpha) \\ &\times \left(\frac{1}{m_1^2} + \frac{Z}{4m_1 m_2} + \frac{Z^2}{m_2^2} \right)^2 \end{aligned} \quad (15)$$

which is approximately 8 KHz for the $2P-2S$ Lamb shift in Hydrogen. Substituting $Z = 1$ and $m_1 = m_2 = m_e$ gives the $\alpha^8 \ln^3 \alpha$ Lamb shift for positronium

$$\Delta E = \frac{3m_e \alpha^8 \ln^3 \alpha}{8\pi^2 n^3}. \quad (16)$$

The positronium Lamb shift is a new result, as are the recoil terms in the Hydrogen Lamb shift. In the limit $m_1/m_2 \rightarrow 0$, the Hydrogen Lamb shift has been computed previously by several groups. There is an analytic computation by Karshenboim [36] and a numerical computation by Goidenko et al. [37] that agree with our result. There are also numerical computations by Malampalli and Sapirstein [38], and by

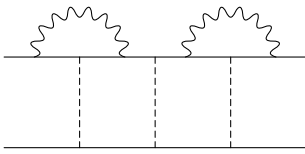


Figure 15. Four-loop diagram that contributes to the $\alpha^8 \ln^2 \alpha$ Lamb shift

Yerokhin [39] which agree with each other, but disagree with the other results. Recently, there has been a computation by Pachucki [40] that agrees with our result. Yerokhin [41] has emphasized that the complete $\alpha^8 \ln^3 \alpha$ Lamb shift might not be contained in the loop-after-loop calculations of Refs. [38,39].

The other calculations rely on extracting the logarithm from four-loop diagrams such as Fig. 15. The velocity renormalization group factors the graph into the product of a two-loop anomalous dimension ρ_{c22} , and the square of a one-loop anomalous dimension γ_0^2 .

11.2. $\ln^2 \alpha$

The $\ln^2 \alpha$ contribution to the hyperfine splitting and decay widths is given by the $U_2(\nu)$ contribution

$$\gamma_0 \rho_{c22} U_c^2(1) [U_2(1) + U_s(1)\mathbf{S}^2] \ln^2 \nu + \dots \quad (17)$$

The spin-dependent term gives the $\alpha^7 \ln^2 \alpha$ hyperfine splitting

$$\begin{aligned} \text{HFS} &= -\frac{64Z^6 \alpha^7 m_R^5 \mu_1 \mu_2}{9m_1 m_2 \pi n^3} \ln^2(Z\alpha) \\ &\times \left[\frac{1}{m_1^2} + \frac{Z}{4m_1 m_2} + \frac{Z^2}{m_2^2} \right] \end{aligned} \quad (18)$$

where μ_i are the magnetic moments normalized to unity for a Dirac fermion. Our result agrees with previous calculations [36,42]. Substituting the matching values for $U_s(1)$ for positronium (which differs from Hydrogen because of annihilation contributions), one finds the positronium hyperfine splitting

$$\text{Ps HFS} = -\frac{7m_e}{8\pi n^3} \alpha^7 \ln^2 \alpha, \quad (19)$$

which agrees with a recent computation of Melnikov and Yelkhovsky [43]. The imaginary parts of the matching coefficients give the decay widths [36],

$$\frac{\Delta\Gamma}{\Gamma_0} = \gamma_0 \rho_{c22} U_c(1)^2 \ln^2 \nu = -\frac{3}{2\pi} \alpha^3 \ln^2 \alpha, \quad (20)$$

for both ortho- and para-positronium.

11.3. $\ln \alpha$

The $\ln \alpha$ contributions to the decay width arise from

$$\begin{aligned} U_{2+s} &\left[\rho_{c22} U_c (U_{2+s} + 2U_r) \right. \\ &\left. + \rho_{cc2} U_c^2 + \rho_{2k} U_k \right] \ln \nu + \dots \end{aligned} \quad (21)$$

which give

$$\begin{aligned} \frac{\Delta\Gamma}{\Gamma_0} &= \left(\frac{m_e^2}{2\pi} \text{Re} U_{2+s} - 2 \right) \ln \nu \\ &= \left(\frac{7\mathbf{S}^2}{6} - 2 \right) \alpha^2 \ln \alpha, \end{aligned} \quad (22)$$

so that

$$\begin{aligned} \left(\frac{\Delta\Gamma}{\Gamma_0} \right)_{\text{ortho}} &= \frac{\alpha^2}{3} \ln \alpha, \\ \left(\frac{\Delta\Gamma}{\Gamma_0} \right)_{\text{para}} &= -2\alpha^2 \ln \alpha. \end{aligned} \quad (23)$$

These agree with existing results [44,45].

12. CONCLUSIONS

The methods presented here give a systematic way of separating scales in nonrelativistic bound state problems. All large logarithms are summed using the velocity renormalization group. The method provides a universal description of QED logarithms. The agreement with known results at order $\alpha^5 \ln \alpha$, $\alpha^6 \ln \alpha$, $\alpha^7 \ln^2 \alpha$, and $\alpha^8 \ln^3 \alpha$ is a highly non-trivial check of the formalism. In QED, one finds that the leading order series terminates after one term, and the next-to-leading order series terminates after three terms. In addition, the method resolves a controversy about the $\alpha^8 \ln^3 \alpha$ Lamb shift for Hydrogen, and gives the first calculation of the $\alpha^8 \ln^3 \alpha$ energy shift for positronium.

In QCD, one can distinguish $\alpha_s(mv)$ and $\alpha_s(mv^2)$, and both can appear simultaneously in the same anomalous dimension. The renormalization group improved potentials can be used to compute $\bar{t}t$ production, and reduce the scale uncertainties by a factor of ten.

The velocity renormalization group should also be applicable to other problems with correlated scales. In the bound state problem, one can generate the scale mv in loop graphs from the scale m and mv^2 , $mv = \sqrt{m \times mv^2}$. Similar effects can occur at finite temperature, where one has the scales T , gT and g^2T , and some of the ideas described here might be applicable to that problem as well.

This work was supported in part by the Department of Energy under grant DOE-FG03-97ER40546 and by NSERC of Canada.

REFERENCES

1. W.E. Caswell and G.P. Lepage, Phys. Lett. **167B** (1986) 437.
2. G.T. Bodwin, E. Braaten and G.P. Lepage, Phys. Rev. **D51** (1995) 1125, Erratum *ibid.* **D55** (1997) 5853.
3. P. Labelle, Phys. Rev. **D58** (1998) 093013.
4. M. Luke and A.V. Manohar, Phys. Rev. **D55** (1997) 4129.
5. A. V. Manohar, Phys. Rev. **D56** (1997) 230.
6. B. Grinstein and I.Z. Rothstein, Phys. Rev. **D57** (1998) 78.
7. M. Luke and M.J. Savage, Phys. Rev. **D57** (1998) 413.
8. A. Pineda and J. Soto, Nucl. Phys. Proc. Suppl. **64** (1998) 428.
9. A. Pineda and J. Soto, Phys. Rev. **D58** (1998) 114011.
10. A. Pineda and J. Soto, Phys. Rev. **D59** (1999) 016005.
11. M.E. Luke, A.V. Manohar, and I.Z. Rothstein, Phys. Rev. **D61** (2000) 074025.
12. A.V. Manohar and I.W. Stewart, Phys. Rev. **D62** (2000) 014033.
13. A.V. Manohar and I.W. Stewart, Phys. Rev. **D62** (2000) 074015.
14. A.V. Manohar and I.W. Stewart, hep-ph/0003107.
15. A.V. Manohar and I.W. Stewart, Phys. Rev. Lett. **85** (2000) 2248.
16. N. Brambilla, A. Pineda, J. Soto and A. Vairo, Nucl. Phys. **B566** (2000) 275.
17. B. A. Kniehl and A. A. Penin, Nucl. Phys. **B563** (1999) 200.
18. S.R. Lundeen and F.M. Pipkin, Phys. Rev. Lett. **46** (1981) 232.
19. H. Hellwig et al. IEEE Trans. **IM-19** (1970) 200.
20. W. Liu et al., Phys. Rev. Lett. **82** (1999) 711.
21. A. Manohar and H. Georgi, Nucl. Phys. **B234** (1984) 189.
22. Quantum Electrodynamics, ed. T. Kinoshita, (World Scientific, Singapore, 1990).
23. K. Pachucki, Hyp. Int. **114** (1998) 55.
24. M.I. Eides, H. Grotch, and V.A. Shelyuto, hep-ph/0002158.
25. A.V. Manohar, J. Soto, and I.W. Stewart, Phys. Lett. **B486** (2000) 400.
26. A.V. Manohar and I.W. Stewart, UCSD/PTH 00-24.
27. A.H. Hoang, A.V. Manohar, I.W. Stewart, and T. Tebuner, UCSD/PTH 00-25.
28. A.H. Hoang, A.V. Manohar, I.W. Stewart, and T. Tebuner, UCSD/PTH 00-26.
29. M. Beneke and V.A. Smirnov, Nucl. Phys. **B522** (1998) 321.
30. H. W. Griesshammer, Nucl. Phys. **B579** (2000) 313.
31. A. Pineda and J. Soto, hep-ph/0007197.
32. A. H. Hoang *et al.*, Eur. Phys. J. direct **C3** (2000) 1.
33. A. H. Hoang, Z. Ligeti and A. V. Manohar, Phys. Rev. Lett. **82** (1999) 277.
34. A. H. Hoang, Z. Ligeti and A. V. Manohar, Phys. Rev. **D59** (1999) 074017.
35. A. H. Hoang and T. Teubner, Phys. Rev. **D60** (1999) 114027.
36. S.G. Karshenboim, Sov. Phys. JETP **76** (1993) 541.
37. I. Goidenko et al., Phys. Rev. Lett. **83** (1999) 2312.
38. S. Mallampalli and J. Sapirstein, Phys. Rev. Lett. **80** (1998) 5297.
39. V. A. Yerokhin, Phys. Rev. **A62** (2000) 012508.
40. K. Pachucki, unpublished.

41. V. A. Yerokhin, hep-ph/0010134.
42. P. Labelle, Ph. D. thesis, Cornell University, 1994 (unpublished).
43. K. Melnikov and A.S. Yelkhovsky, Phys. Lett. **B458** (1999) 143.
44. W.E. Caswell and G.P. Lepage, Phys. Rev. **A20** (1979) 36.
45. I.B. Khriplovich and A.S. Yelkhovsky, Phys. Lett. **B246** (1990) 520.